

Design of Non-linear Beam-type Spring for Designated Loading and Displacement for Use in Lower-limb Orthosis

Dein Shaw^{1,2}, Chih-Ren Huang² and Li-Cheng Huang²

Abstract: In this study, a method for designing an in-plane, free-form, beam-type spring for use in a lower-limb orthosis was developed. A spring designed by this method follows a predefined relationship between loading and displacement. To facilitate the analysis of the spring, it was divided into several beam segments. The stiffness equations related to loading (including moment and force) and displacements (linear and rotation) of each beam segment were found to follow a modified (non-linear) Castigliano's second theorem (NCST) and were assembled by using the continuity of nodal points of neighbouring curve segments. Using the proposed method, a spring designer can design the spring which has the relationship between the loading and displacement of springs such as those used in lower-limb orthoses. In order to verify the effectiveness of the proposed method, analysis results of deformation of a cantilever spring and cubic spline spring by the finite element method, Castigliano's second theorem, and NCST were compared. Further, an experiment was performed in which the path of motion of the lower limb of a subject climbing up stairs was measured. The results showed that the proposed method was effective and NCST could be successfully used to design the shape of the cubic spline spring.

Keywords: Spring design, non-linear beam, Castigliano's second theorem, spring structures.

1 Introduction

Different types of springs are employed in different applications, and each spring usually has a spring constant. An example of use of a spring is in a lower-limb orthosis. A patient with osteoarthritis of the knee, in addition to undergoing medical treatment, must wear a lower-limb orthosis to lighten the burden at the knee joint.

¹ Tel.: + 886-3-5715131 ext. 42604; Fax: + 886-3-57339979; E-mail: dishaw@pme.nthu.edu.tw

² Department of Power Mechanical Engineering, National Tsing Hua University, Hsin Chu, Taiwan, R.O.China

Designs of these orthoses vary depending on patient requirements. Most orthotic knee joints are designed as pin joints or as a simple linkage joint to support the rotational motion of the knee [Sawicki, Gordon, and Ferris (2005)], and a motor is used to power the lower-limb orthosis. In reality, the motion of the human knee joint includes rolling and sliding in addition to rotational motion. The pin joint or simple linkage joint does not permit smooth movement of the knee joint. Such conflicting motion between the orthosis joint and the knee joint causes discomfort to the patient. Therefore, the movement of the joint of the orthosis joint should be designed such that it ensures smooth movement of the patient's knee joint. In this study, a method for designing a non-linear beam-type spring of the lower-limb orthosis was developed. The relationship between the external forces (including moments) and displacements (including angles) in this study is constrained by the motion requirement of the patient.

2 Theoretical background and proposed method

Several energy methods have been developed [Cook and Young (1999)] for calculating the displacement (or deflection) of a structure under loads; examples include the virtual work method, the unit load method, a method employing Castigliano's second theorem, the Rayleigh-Ritz method, and the finite element method (FEM) [Panthi, Ramakrishnan, Pathak and Chouhan (2007)]. In fact, some of these methods are similar in nature, the main difference between them being the way in which they address the problem. These differences are explained as follows. Under the static equilibrium condition, the virtual work method involves a state in which the virtual work due to virtual displacements is always zero; this state can be used to determine the relation between load and displacement. In the unit load method, the equation of virtual work due to a unit load is used to obtain the displacement of a structure at the position of the unit load. Further, Castigliano's second theorem states that displacement is equal to the first partial derivative of the strain energy with respect to loads. The principle of the unit load method is similar to Castigliano's second theorem. In the unit load method, it is essential to assign the correct sign to each term; however, in Castigliano's second theorem, the sign is not important (because the energy contains square terms). By the Rayleigh-Ritz method, the minimum stationary potential energy state is sought and a displacement or displacement equations prefaced by this state are determined. In recent times, many kinds of solution methods are being developed by using the FEM [for example, Pu, Zhihai, Xiasong, Guorong, Xiaoqin and Zhangzhi (2009)]. The fundamental concept of the FEM is to divide the model into a limited number of elements, each of which has several nodal points. Each nodal point has several degrees of freedom (DOF) of displacement. The calculus of the variation method together

with the nodal DOF is used to determine the stiffness matrix of each element. After assembly this stiffness matrix of every elements, all the nodal DOF and suitable boundary conditions and external loads are applied, the displacement of the nodal point can be calculated (the mean time stress and strain are also calculated).

A free-form curve can be drawn in several forms such as the cubic spline (CS) curve, Bézier curve, B-spline curve, and rational curve [Piegl and Tiller (1995); Rogers (2001)]. A CS curve is composed of several third-degree piecewise polynomial curves. The CS curve has a second-order continuity of derivatives. For this curve, end conditions at both end points must be specified, and curves can usually be represented as implicit equations or parametric functions [Zeid (1991); Burden and Faires (2001)].

A Bézier curve is defined in terms of several control points. Only the first and last of the control points of a polygon actually lie on the curve. A B-spline curve is a powerful generation of Bézier curves. B-spline curves can be used to interpolate or approximate a set of given data points. The curves are constructed by several basic (blending) functions. The rational curve is an improvement of the Bézier curve or B-spline Curve. The most widely used rational curve is the non-uniform rational B-spline (NURBS) curve.

Out of all these curves, the CS curve is most effective in describing a planar curve with nodal points having unknown locations. Therefore, the CS curve was used to form the shape of the spring in this study. The deformation of free-form curve beams has not been well researched. Gontier and Vollmer (1995) proposed an interesting method to solve the deformation problem of beams in the form of a Bézier curve. In their study, the deformation of the structure was under large rotation.

In this study, the beam to be designed is divided into several small beams with unknown initial end-point positions. The equations related to loading (including moment and force) and displacement (including displacement and rotation) for each beam can be set up by using Castigliano's second theorem. The equations of each beam are connected by using the displacement continuity of nodal points. It is noted that due to the shape of the spring is to be determined, and the CS curve is used to form the beam-type spring; therefore, the control points of the beam-type spring are the parameters to be determined.

When designing the beam-type spring, the relative positions of both ends of the spring for different external loads are first determined according to the design requirements. Then, these relations are input into the governing equations to obtain several non-linear equations of the unknown nodal points of the beams that are used to construct the spring. Solving the nonlinear equations yields the positions of the unknown nodal points. The nodal points are then treated as the control points of

the CS curve. By using these control points and the equation of the CS curve, a beam-type spring that has the required load-displacement curve is obtained.

2.1 Derivation of governing equations

The orthosis designed in this study comprises a beam-type spring joint, upper and lower frame structures, and an air muscle powered by a pneumatic muscle (configuration shown in Fig. 1). Force F_{a-m} shown in Fig. 1 is generated by the air muscle. The relative movement between the upper and lower frame structures follows the relative movement of the patient's thigh and calf.

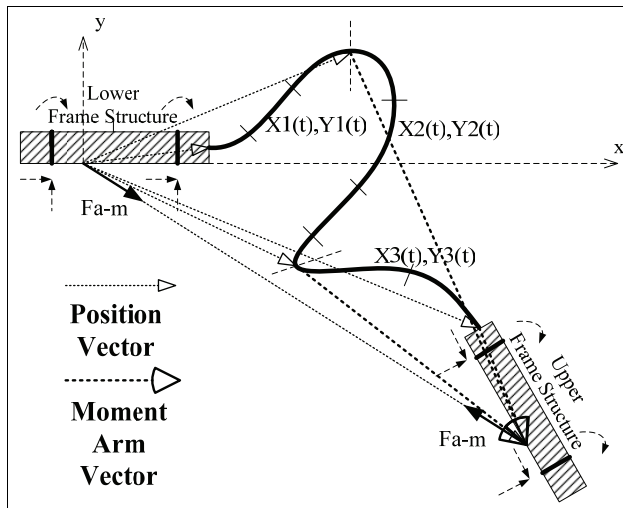


Figure 1: Configuration of free-form beam-type spring

As shown in Fig. 1, the spring is constructed using three CS curves. The only constraint in each of these curves is the continuity of displacement. However, in the design process, the beam-type spring is analyzed using a straight beam.

2.2 Derivation of non-linear beam equation using Castigliano's second theorem

The equation of Castigliano's second theorem used to analyze the spring is expressed as follows:

$$\delta_i = \frac{\partial U^*}{\partial F_i} \quad (1)$$

Here, U^* is the complementary energy of the structure and δ_i is the generalized displacement at the i th point where the load F_i is applied. The generalized loads include the force, bending moment, and torque. The generalized displacements include displacements, rotation angles, and torsion angles. However, when the relation between σ (stress) and ε (strain) is linear, then $U^* = U$ (where U is the strain energy), and Eq. (1) becomes:

$$\delta_i = \frac{\partial U}{\partial F_i} \quad (2)$$

In this study, we assumed that the cross section of the beam is uniform and that the beam material is linear and isotropic. The Castigliano's theorem was developed in the framework of a beam subjected to small strain and large rotation. According to the energy method, strain energy can be expressed by using forces and moments [Cook and Young (1999)]:

$$U = \int \frac{N N dx}{2 EA} + \frac{T T dx}{2 GK} + \frac{M_y M_y dx}{2 EI_y} + \frac{M_z M_z dx}{2 EI_z} + \frac{V_y k_y V_y dx}{2 GA} + \frac{V_z k_z V_z dx}{2 GA} \quad (3)$$

Here, N is the axial force; T is the torsion; M_y and M_z are the bending moments and V_y and V_z are the shear forces in the y and z directions, respectively; E is the Young's modulus; G is the shear modulus; A is the cross-sectional area of the beam; and I_y and I_z are the moments of inertia of the beam in the y and z directions, respectively. Because the cross section is assumed to be uniform, the torsion effect can be eliminated from Eq. (3), and then, the strain energy becomes

$$U = \int \left(\frac{N N}{2 EA} + \frac{M_z M_z}{2 EI_z} + \frac{V_y k_y V_y}{2 GA} \right) dx \quad (4)$$

Eq. (4) contains only axial force, bending moment, and shear force terms.

By using Eq. (2), Eq. (4) becomes

$$\delta_i = \frac{\partial U}{\partial F_i} = \int \left(\frac{N}{EA} \frac{\partial N}{\partial F_i} + \frac{M}{EI} \frac{\partial M}{\partial F_i} + \frac{kV}{GA} \frac{\partial V}{\partial F_i} \right) dx \quad (5)$$

Here, δ_i can be the displacement δ or rotation angle θ , and F_i can be the applied load or applied moment. Eq. (5) can be used to derive the equations for calculating the displacement and angle. However, Castigliano's second theorem is always used for the analysis of linear structures. The equation of this theorem must be modified if it is to be used for analysis of non-linear structures. In this study, we also assumed that the spring is a wire spring and is under small strain and large rotation. These

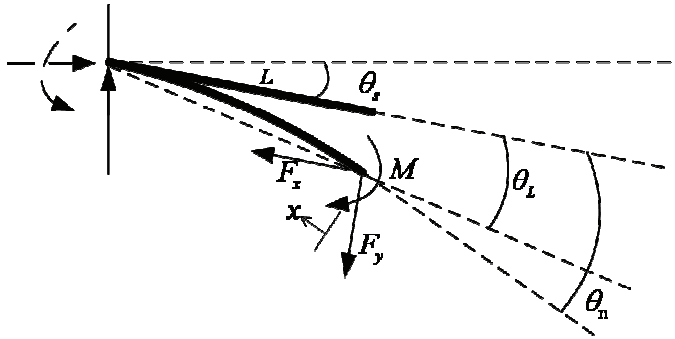


Figure 2: Configuration of beam element

assumptions allow each small section of the spring to be treated as a linear segment.

As shown in Fig. 2, two forces and one bending moment are applied to a cantilever beam of length L . The left end of the beam forms an angle θ_s with the horizontal axis. The deformations at the end of the beam include a rotation angle θ_n . If we do not consider the influence of curvature on shortening, the length in the x direction remains L at any load. The end-point-to-end point angle θ_L is shown in Fig. 2. If L is sufficiently small, $\theta_L \approx \frac{1}{2} \times \theta_n$. If a more precise equation is required, then the effect of length change along the x direction should be considered. If only the moments produced by the axial force and shear force and the applied moment in Eq. (5) are considered, the governing equation will become as shown in Eq. (6). In Eq. 6, the strain energies of the axial and shear forces (i.e. the first and third terms of Eq. (5)) are neglected because the magnitudes of these energies are much smaller than the bending moment.

$$\theta_n = \frac{1}{EI} \int_0^L [F_x x \sin(\theta_s + \frac{\theta_n}{2}) + F_y x \cos(\theta_s + \frac{\theta_n}{2}) + M] dx \quad (6)$$

In order to demonstrate the method of using Eq. (6), a beam composed of three segments, shown in Fig. 3, is used as an example. The equations of each segment are as follows:

$$\theta_{n3} = \frac{1}{EI} \int_0^{L_3} [F_{3x} x \sin(\theta_3 + \theta_{s3} + \frac{\theta_{n3}}{2}) + F_{3y} x \cos(\theta_3 + \theta_{s3} + \frac{\theta_{n3}}{2}) + M_3] dx \quad (7)$$

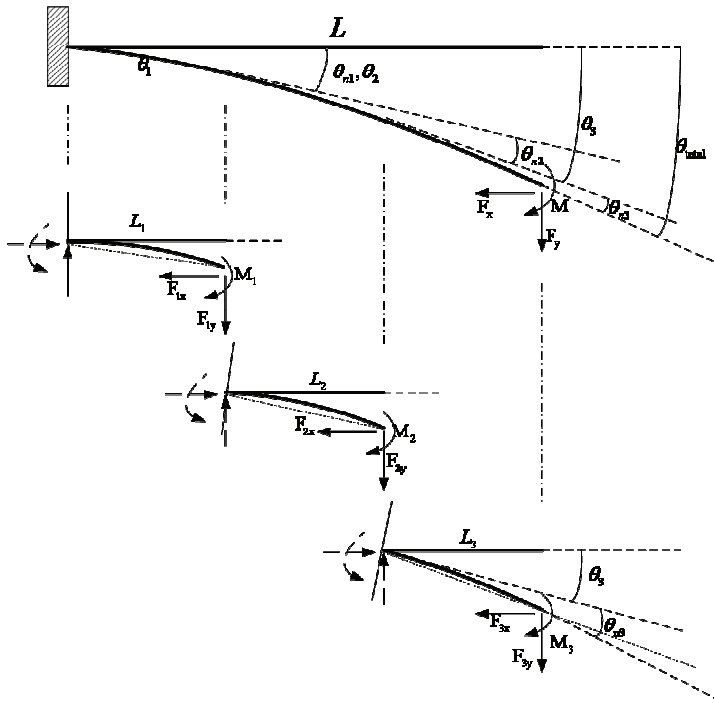


Figure 3: Configuration of beam divided into three elements

$$\theta_{n2} = \frac{1}{EI} \int_0^{L_2} [F_{2x}x \sin(\theta_2 + \theta_{s2} + \frac{\theta_{n2}}{2}) + F_{2y}x \cos(\theta_2 + \theta_{s2} + \frac{\theta_{n2}}{2}) + M_2] dx \quad (8)$$

and

$$\theta_{n1} = \frac{1}{EI} \int_0^{L_1} [F_{1x}x \sin(\theta_1 + \theta_{s1} + \frac{\theta_{n1}}{2}) + F_{1y}x \cos(\theta_1 + \theta_{s1} + \frac{\theta_{n1}}{2}) + M_1] dx \quad (9)$$

where

$$\theta_{total} = \theta_{n1} + \theta_{n2} + \theta_{n3}$$

and

$$F_{1x} = F_{2x} = F_{3x} = F_x(n_3, \theta_{n3}), \quad F_{1y} = F_{2y} = F_{3y} = F_y(n_3, \theta_{n3})$$

The end-point coordinates of nodes 1–3 can be expressed as

$$\begin{aligned}
 n_3 &= n_1 + n_2 + [L_3 \cos(\theta_{s1} + \theta_{n1} + \theta_{s2} + \theta_{n2} + \theta_{s3} + \frac{\theta_{n3}}{2}), \\
 &\quad L_3 \sin(\theta_{s1} + \theta_{n1} + \theta_{s2} + \theta_{n2} + \theta_{s3} + \frac{\theta_{n3}}{2})] \\
 n_2 &= n_1 + [L_2 \cos(\theta_{s1} + \theta_{n1} + \theta_{s2} + \frac{\theta_{n2}}{2}), L_2 \sin(\theta_{s1} + \theta_{n1} + \theta_{s2} + \frac{\theta_{n2}}{2})] \\
 n_1 &= [L_1 \cos(\theta_{s1} + \frac{\theta_{n1}}{2}), L_1 \sin(\theta_{s1} + \frac{\theta_{n1}}{2})]
 \end{aligned} \tag{10}$$

The boundary conditions of the moment at each end point are

$$\begin{aligned}
 M_3 &= M(n_3, \theta_{n3}) \\
 M_2 &= F_{3x}L_3 \sin(\theta_3 + \theta_{s3} + \frac{\theta_{n3}}{2}) + F_{3y}L_3 \cos(\theta_3 + \theta_{s3} + \frac{\theta_{n3}}{2}) + M_3 \\
 M_1 &= F_{2x}L_2 \sin(\theta_2 + \theta_{s2} + \frac{\theta_{n2}}{2}) + F_{2y}L_2 \cos(\theta_2 + \theta_{s2} + \frac{\theta_{n2}}{2}) + M_2
 \end{aligned} \tag{11}$$

In this case, all θ_s are zero. The unknown parameters are θ_{ni} , L_1 , L_2 , and L_3 . L_1 , L_2 , and L_3 are unknown and can be obtained from the coordinates of the nodal points. The relation between the coordinates (position and rotation) of the last end point and the applied forces (in this case, the last end point is located at n_3 ; the rotation is θ_{n3} ; and the applied forces are $F_x(n_3, \theta_{n3})$, $F_y(n_3, \theta_{n3})$, and $M(n_3, \theta_{n3})$) are known functions. Once the unknown parameters are known, the designing of the spring would be completed. Eqs. (7)–(9) can be extended to more elements to simulate more complicated problems. However, these equations are non-linear. Therefore, iteration is carried out to obtain the results.

3 Verification of proposed method

3.1 Analysis of straight beam

In this section, we present a comparison of beam analysis results obtained using a nonlinear Castigliano’s Second Theorem (NCST), Castigliano’s second theorem, and the FEM (used in cases of cantilever beam deformation) in order to verify the effectiveness of the proposed method. The NCST results include the results of two cases—of using one element and of using three elements.

The finite element software ANSYS (ANSYS Workbench 10) was used to simulate large deformations of the cantilever beam. The finite-element mesh was generated automatically by applying loads (lateral load, axial load, and moment) at the free end. ANSYS mesh controls are also available. The element size was determined by the proximity of other topologies, body curvature, and complexity of the beam.

The beam was made of stainless steel; the mechanical properties of stainless steel are and $\nu = 0.33$. The dimensions of the beam were assumed to be and, where D is the diameter.

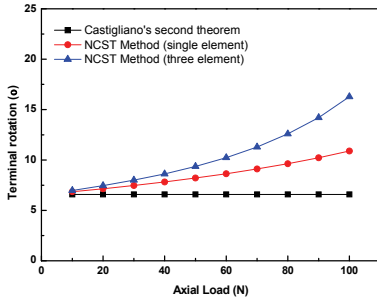


Figure 4: Results of NCST, Castigliano's second theorem, and finite element method

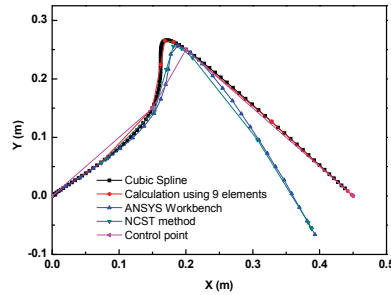


Figure 5: Results of analysis of free-form spring by ANSYS Workbench and NCST

The beam was loaded with a lateral load (10 N), a moment load (1 N-m), and an axial load (varied from 10 N to 100 N) at the free end of the cantilever beam. The results of analysis are shown in Fig. 4. In this figure, the black line shows the results of Castigliano's second theorem, the red line shows the NCST results for a single element, and the blue line shows the NCST results for three elements; in this case, the rotation angle was 16.3° . The red circle represents the results of the FEM. In this case, the rotation angle was 17.5° . That is, the difference between these rotation angles was 1.2° . However, after increasing the number of elements, the rotation angle calculated by the FEM became 17.3° . These results show that the proposed method is sufficiently effective for simulating a beam with a large rotation angle.

3.2 Analysis of free-form spring

The material properties of a free-form spring, shown in Fig. 5, were and $\nu = 0.33$. The diameter of the beam was 0.006 m. The shape of the free-form spring was determined by four control points (magenta line) and by the slope of the load point, as shown in Fig. 5. The external loads applied to the beam were a lateral load of 25 N and a moment load of 1 N-m. The black line in Fig. 5 represents the shape of the free-form spring; the red line shows the configuration of elements of the beam in the case of using NCST.

Fig. 5 shows the results of the analysis of the free-form spring by ANSYS and NCST, calculated by using nine elements (red line). The blue and green lines in this figure show the results obtained using ANSYS Workbench and NCST, respectively. Thus, it can be observed that the results of NCST agree with those of ANSYS.

4 Design algorithm

This section describes the following parts of the study: measurement of the path of motion of the lower limb of a subject while climbing stairs and design of the spring by using the measurement data obtained in the first part.

4.1 Determination of relation between load and displacement of orthosis

A 26 year old male (weight: 60kg, height: 180 cm) participated in the study. The lower-limb motion of the subject while climbing stairs was measured using a 3D-space system (Vicon Motion Systems, Ltd., Oxford, UK). The subject did not have any history of injury, trunk disorder, or lower-limb disorder that would affect his gait. The height of the stairs was 23 cm for the first stage and 49 cm for the second stage, as shown in Fig. 6. The measured motion data were used as the input for LifeMOD (biomechanics simulation software). This software was used to simulate the path of the lower limb and forces generated in the human body, whose measurement is otherwise difficult [Shaw and Huang (2006)].

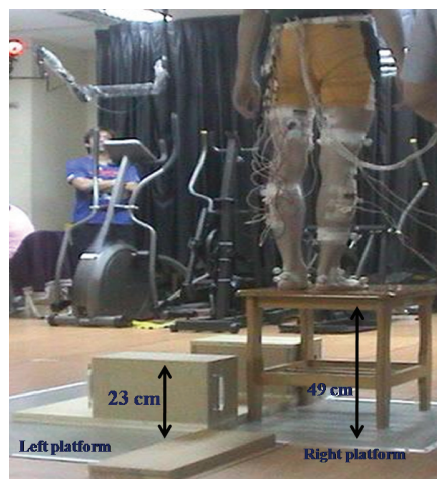


Figure 6: Experimental setup showing 3D positions of markers

Fig. 7(a) shows a LifeMOD-simulated image of the motion of climbing stairs. Fig. 7(b) shows the simulated path of the markers on the thigh and shank. In Fig. 7(b),

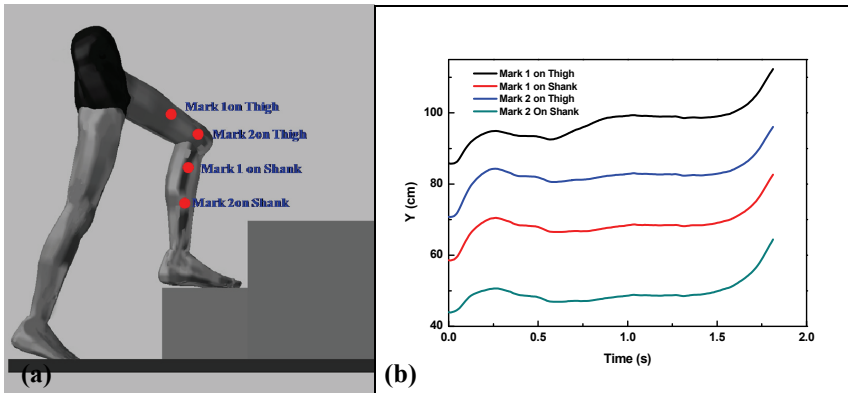


Figure 7: (a) LifeMOD-simulated image of climbing stairs and (b) Paths traced by markers on thigh and shank while climbing stairs

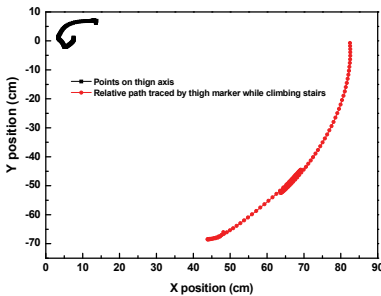


Figure 8: Relative path of motion between thigh and shank during stair climbing

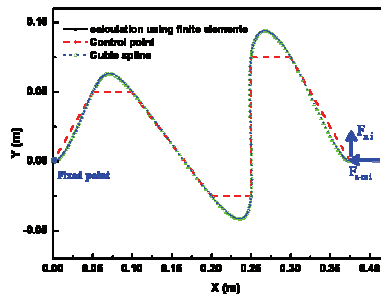


Figure 9: Shape of beam-type spring with applied axial load (F_{a-mi}) and lateral load (F_{ni})

the black and blue lines represent paths of the markers of the thigh and the red and dark cyan lines represent those of the shank. Fig. 8 shows the relative path of motion between the thigh and the shank. Using the data shown in Fig. 7(b), the paths of the markers on the thigh and left lower limb can be determined. In Fig. 6, the black line shows the positions of the shank axis, and the red line shows the relative path of the thigh and shank. This relative path was used to evaluate the comfort level of individuals who use beam-type springs. The measured (and simulated) load and relative motion path can be used to design the spring joint of

the orthosis.

4.2 Design of beam-type spring

As shown in Eqs. (7)–(9), the forces and moment are a function of the location of the last end point; therefore, in order to solve these equations, one should divide the forces into several consequent load steps; this division ensures that there are sufficient equations to determine the unknown coordinates of each nodal point. This implies that the external forces are $F_x(n_{nN}, \theta_{nN})$, $F_y(n_{nN}, \theta_{nN})$, and $M(n_{nN}, \theta_{nN})$. For each force step, the corresponding rotation angles at the nodal points should be determined and grouped appropriately. For each step, the governing equations (Eqs. (7)–(9)) have the same form, except for different rotation angles and external forces. By this procedure, the number of equations becomes equal to the unknown nodal degree of freedom. The non-linear equations are solved iteratively to determine all unknown parameters.

According to the actuating loads and required moment, the first set of actuating loads is fixed to $F_{a-m1}(F_x) = 0$ and $F_{n1}(F_y) = -4.5$ N; the second set of actuating loads is fixed to $F_{a-m2} = 20$ N and $F_{n2} = -34$ N; and the third set of actuating loads is fixed to $F_{a-m3} = 47$ N and $F_{n3} = -30$ N. The beam-type spring is divided into eight control points to form the free-form spring. The shape of the spring is shown in Fig. 9.

The beam-type spring is designed by using the eight control points to form the shape of a CS spring. This beam-type spring is initially assumed to be M-shaped according to the properties of the end-point movement required by human motion. However, 21 nodal points on the CS curve are used in NCST to determine the shape of the beam-type spring.

Fig. 10 shows the deformation results for different actuating loads on the beam-type spring. In this figure, in this figure, the black, red, and blue lines show the deformation results for the first, second, and third sets of actuating loads, respectively

These actuating loads have different deformations under different loads. Moreover, this deformation agrees with the relative path traced by the subject while climbing stairs (in Fig. 10, see the magenta line and dark cyan line (reference circle)).

5 Conclusions

In this study, a method for designing a non-linear beam-type spring of the lower-limb orthosis was developed. The spring designed by this method follows a pre-defined relationship between loading and displacement. The developed method accounts for the effect of the moment, transverse load, and axial load of a beam. Finally, a method employing a non-linear Castigliano's second theorem was devel-

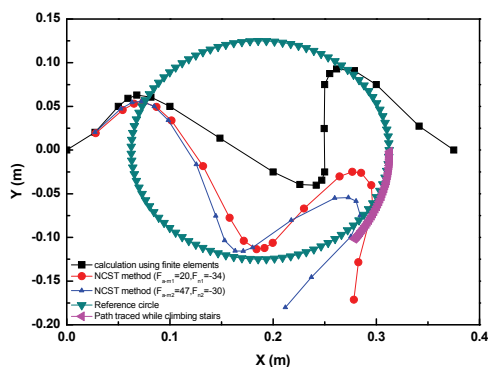


Figure 10: Deformation results for different actuating loads applied to beam-type spring

oped. Calculation results of deformation of a cantilever beam and a cubic spline spring by ANSYS Workbench and NCST were found to be in agreement.

Further, an experiment was performed for measuring the relative movement of the thigh and shank of a subject wearing a lower-limb orthosis while climbing up stairs; as a result, the relative path of the subject's motion was obtained. The forces generated in the subject's body were also measured. The software LifeMOD was used to simulate the motion and forces that could not be measured experimentally. The simulation results indicated that the relative movement between the thigh and shank follows an approximately elliptical path. Finally, the design results indicated that the NCST could be successfully used to design the shape of the cubic spline spring.

References

- Burden, R. L.; Faires, J. D.** (2001): *Numerical Analysis*, seventh ed., Brooks/Cole.
- Cook, R. D.; Young, W. C.** (1999): *Advanced Mechanics of Materials*, second ed., Prentice-Hall.
- Gontier, C.; Vollmer, C.** (1995): A large displacement analysis of a beam using a CAD geometric definition. *Computers & Structures*, vol. 57, no. 6, pp. 981–989.
- Panthi, S. K.; Ramakrishnan, N.; Pathak, K. K.; Chouhan, J. S.** (2007): Prediction of Springback in Straight Flanging using Finite Element Method. *CMC: Computers Materials & Continua*, vol. 6, no. 1, pp. 13–20.
- Piegl, L.; Tiller, W.** (1995): *The NURBS Book*. Springer-Verlag.

Pu, Y.; Zhihai, X.; Xiasong, H.; Guorong, L.; Xiaoqin, Z. H. M.; Zhangzhi, C. (2009): Limit Load of Soil-Root Composites. *CMC: Computers Materials & Continua*, vol. 10, no. 2, pp. 117–137.

Rogers, D. F. (2001): *An Introduction to NURBS: With Historical Perspective*. Academic Press.

Sawicki, G. S.; Gordon, K. E.; Ferris, D. P. (2005): Powered lower limb orthoses: Applications in Motor Adaptation and Rehabilitation. *Proceedings of the IEEE 9th International Conference on Rehabilitation Robotics*, Chicago, USA.

Shaw, D.; Huang, C. R. (2006): Analysis of lower limb orthosis while climbing the stair. *International Symposium on Biomedical Engineering*, Taiwan.

Sen Yung Lee; Shin Yi Lu; Yen Tse Liu; and Hui Chen Huang (2008): Exact Large Deflection Solutions for Timoshenko Beams with Nonlinear Boundary Conditions. *CMES: Computer Modeling in Engineering & Sciences*, Vol. 33, No. 3, pp. 293-312.

Zeid, I. (1991): *CAD/CAM Theory and Practice*. McGraw Hill.